



HAL
open science

Modélisation et Simulation de Francis Turbine Inter-blade Vortices in Partial Load Conditions

Sofien Bouajila, James Brammer, Emmanuel Flores, Claire Ségoufin, Thierry
Maître

► **To cite this version:**

Sofien Bouajila, James Brammer, Emmanuel Flores, Claire Ségoufin, Thierry Maître. Modélisation et Simulation de Francis Turbine Inter-blade Vortices in Partial Load Conditions. Congrès SHF : “SIMHYDRO 2017”, Jun 2017, Nice, France. hal-01905964

HAL Id: hal-01905964

<https://hal.science/hal-01905964>

Submitted on 26 Oct 2018

HAL is a multi-disciplinary open access archive for the deposit and dissemination of scientific research documents, whether they are published or not. The documents may come from teaching and research institutions in France or abroad, or from public or private research centers.

L'archive ouverte pluridisciplinaire **HAL**, est destinée au dépôt et à la diffusion de documents scientifiques de niveau recherche, publiés ou non, émanant des établissements d'enseignement et de recherche français ou étrangers, des laboratoires publics ou privés.

MODELISATION AND SIMULATION OF FRANCIS TURBINE INTER-BLADE VORTICES IN PARTIAL LOAD CONDITONS

Sofien Bouajila¹, James Brammer, Emmanuel Flores, Claire Ségoufin, Thierry Maître
Mailing addresses

sofien.bouajila@grenoble-inp.org, james.brammer@ge.com, emmanuel.flores@ge.com,
claire.segoufin@ge.com, thierry.maitre@legi.grenoble-inp.fr

KEY WORDS

Off-design operation, dynamic loading, reduced scale test rig measurements, high-speed visualization, URANS calculations.

ABSTRACT

As it is a modern market requirement that hydro-electric power plants become more flexible, hydraulic turbine manufacturers are requested to extend the operating range of their machines. For single regulated Francis turbines, consequent off-design conditions involve more complex flows than the ones of the classical continuous operating range. During partial load operation, several hydraulic phenomena are known to occur in the machine. One of them is the development of inter-blade vortices in the runner, and concerns especially low head turbines. Due to these complex flows, the machines are operated with higher levels of dynamic stresses in the runner that can potentially lead to a premature damage of existing units. Therefore, a better understanding of partial load flows in Francis turbines is required to provide new appropriate designs. To describe the full-size machine behavior, numerical simulations and test rig measurements are used in a complementary way during the design stage. Therefore, new CFD modelisation and experimental techniques are required to address off-design operation. In this study, a reduced scale model of a low head Francis turbine was tested. It was equipped with on-board strain gauges and pressure sensors, in addition to the classical instrumentation. High-speed visualizations of the flow at the inlet of the runner channels were performed by means of three special guide vanes. The experimental data were used to validate numerical simulations of the flow inside the runner. URANS calculations were performed using a commercial code. At partial load conditions, the location of the inter-blade vortices was successfully simulated and the comparison between numerical and experimental results showed a good agreement. The present test rig measurements campaign and numerical simulations are providing further insights about partial load flows inside low head Francis turbine runners.

1. INTRODUCTION

The hydro power industry is transforming due to new needs of the electricity grid. With the integration of renewable energies such as wind and solar, hydro power units are required to be more flexible. To cope with hydro power plants operators demands, hydraulic turbine manufacturers are extending their machines operating ranges. In the case of Francis turbines, new off-design conditions lead to various unsteady hydraulic phenomena that are potentially increasing the level of dynamic loading on the machines. Consequently, increased fatigue damage is expected and needs to be considered in order to avoid premature maintenance operations on the units.

Concerning partial load operation, continuous operating range limits have been stretched in recent years. As the helicoidal vortex rope that develops in the draft tube has been largely investigated, knowledge about the mechanical impact on the runner is providing help at the design stage [1]. From deep partial load to no-load condition, strain fluctuation measurements on reduced scale models provide useful feedback of the dynamic loading on the runner [2] [3] and evidence higher fatigue damage to be expected [4]. However, the hydraulic phenomena that occur in such conditions and their impact on the mechanical loading are not fully understood.

¹ Corresponding author

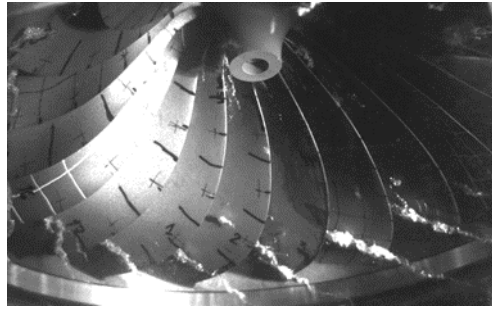


Figure 1: Example of inter-blade vortices occurring during deep partial load operation of a Francis runner

Among these potential root causes, inter-blade vortices (**Figure 1**) are known to develop in the runner channels in deep partial load conditions [5]. This phenomenon has been more studied recently, from its incipient to its more developed forms, based on both experimental and numerical approaches [6] [7] [8]. Nevertheless, the specific impact of inter-blade vortices on the runner mechanical loading remains unclear, as multiple frequency signatures appear to be involved at deep partial load [4]. Strain fluctuation measurements on the runner were performed in [3] and appeared to be poorly correlated with the classical peak-to-peak value of pressure fluctuations in the stationary parts of the turbine.

In the context of design improvement, partial load fatigue damage on the full-scale Francis turbine needs to be estimated, which means that the dynamic loading on the runner needs to be correctly predicted. Therefore, transient pressure fields applied on the runner are required and have to be properly estimated. As numerical simulations of the unsteady and complex flows occurring at deep partial load need to be performed, numerical modelling is used in order to achieve affordable computational costs. Hence, experimental data are essential to validate numerical models and tests on reduced scale machines are performed in deep partial load operating conditions, implying the need for new measurements and visualization techniques.

In this study a low head Francis turbine was tested using a reduced scale model, and CFD simulations were also carried out. The physical model was equipped with on-board strain gauges and pressure sensors, in addition to the classical instrumentation. High-speed visualizations of the flow at the inlet of the runner channels were performed by means of three special guide vanes. Simultaneous strain and pressure measurements are compared to the observations of the inter-blade vortices developing in the runner. The experimental data were compared to URANS simulations of the flow inside the runner.

2. EXPERIMENTAL INVESTIGATION

2.1 Experimental setup

2.1.1 Reduced scale model

A reduced scale model of a low head Francis turbine was used to investigate partial load conditions. Tests were conducted at GE Renewable Energy's Hydraulic Laboratory, in Grenoble. This runner was manufactured to ensure both mechanical and hydraulic similitudes with the full scale machine. In addition to the classical instrumentation recommended by IEC 60193 [9], on-board strain gauges and pressure sensors were placed on the runner (**Figure 2**). Strain gauges are located close to the critical areas where higher levels of dynamic stress are expected, at the blades connections to the crown and the band of the runner. Pressure sensors were positioned at the inlet of one inter-blade channel, on pressure and suction sides of the blades.

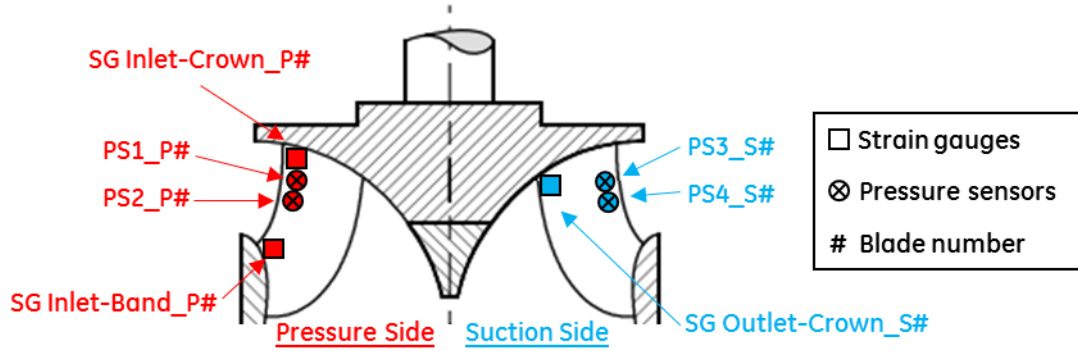


Figure 2: Schematic view of runner on-board instrumentation

2.1.2 Special observation guide vanes

In order to unveil the link between inter-blade vortices, pressure fluctuations in the flow and strain fluctuations in the runner, instrumented guide vanes were specially designed. The purpose of the device is to observe the runner inlet and the inter-blade channel to understand how inter-blade vortices form, develop and evolve during the turbine operation. This is a new visualization technique that has only been used previously on one other case [10], and therefore offers a unique insight of the runner behavior.

In this study, three successive guide vanes of the distributor are instrumented (Figure 3a). The observation guide vane (the middle one) is equipped with a rigid borescope. The instrument goes inside the guide vane through its rotation axis. The middle of the guide vane is made of acrylic glass, and is reproducing the same hydraulic profile as the other guide vanes. To observe the runner inlet, a high-speed camera is connected to the borescope. The two other guide vanes are used to provide continuous lighting inside the runner channels. They are equipped with LED arrays, fixed inside the body of the guide vanes. Again, acrylic glass is used for sealing the electronic components, and ensures the continuity of the hydraulic profiles. Downstream the runner, classical observation technique is implemented: stroboscopic lighting and standard camera are used to capture the flow through the transparent cone of the draft tube. Grid patterns were drawn at the inlet (Figure 3b) and outlet (Figure 3c) of the runner, in to order to easier locate expected hydraulic phenomena.

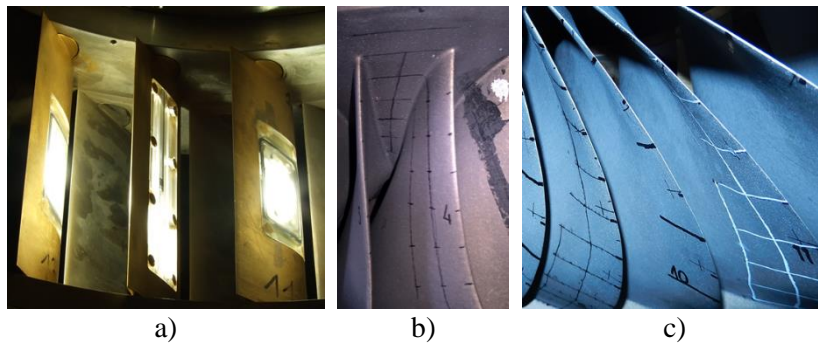


Figure 3: Special guide vanes (a), and Grid pattern to help observations of the flow (b,c)

2.2 Results and observations

The reduced scale model was tested at the rated head and downstream atmospheric pressure (leading to high value of the cavitation number). Dimensionless parameters are used to describe hydraulic turbines hill chart [9]:

$$\begin{array}{lll} \text{Energy coefficient: } \psi = \frac{2gH_n}{(\omega D/2)^2} & \text{Discharge coefficient: } \varphi = \frac{Q}{\pi\omega(D/2)^3} & \text{Torque coefficient: } \tau = \frac{2T_m}{\rho\pi\omega^2(D/2)^5} \end{array}$$

with ρ the density of water ($\text{kg}\cdot\text{m}^{-3}$), g the gravitational acceleration ($\text{m}\cdot\text{s}^{-2}$), H_n the net head (m), Q the discharge ($\text{m}^3\cdot\text{s}^{-1}$), ω the runner rotation speed ($\text{rad}\cdot\text{s}^{-1}$), T_m the runner torque (N.m) and D the reference diameter of the runner (m).

In **Figure 4** the evolution of pressure and strain fluctuations during a load variation is considered. Four pressure sensors were located in the runner (blue), one in the vaneless area (green) and one in the draft tube cone (red). The strain gauges that were used were located at the runner inlet (green) and outlet (orange). Between $0.7\varphi_{opt}$ and $0.9\varphi_{opt}$, a first increase of pressure and strain fluctuations can be seen. It is due to the helicoidal vortex rope that forms in the draft tube. Maximum pressure fluctuations are located in the draft tube, and maximum dynamic strain is found at the outlet of the runner, near the crown. As the discharge decreases, a significant reduction in the dynamic strain is observed straight after the peak, because the vortex rope is no longer a coherent structure. For lower flow rates, fluctuations tend to increase again. At around $0.36\varphi_{opt}$, the runner pressure sensor PS3_S2 shows a first maximum of fluctuations, not observed on the others pressure measurements. At around $0.32\varphi_{opt}$ a sudden increase of the dynamic strain occurs in the runner (from inlet to outlet). The increase is captured by three pressure sensors in the runner. Whilst the fluctuations also rise in the vaneless area this phenomenon cannot be seen from the sensor in the cone.

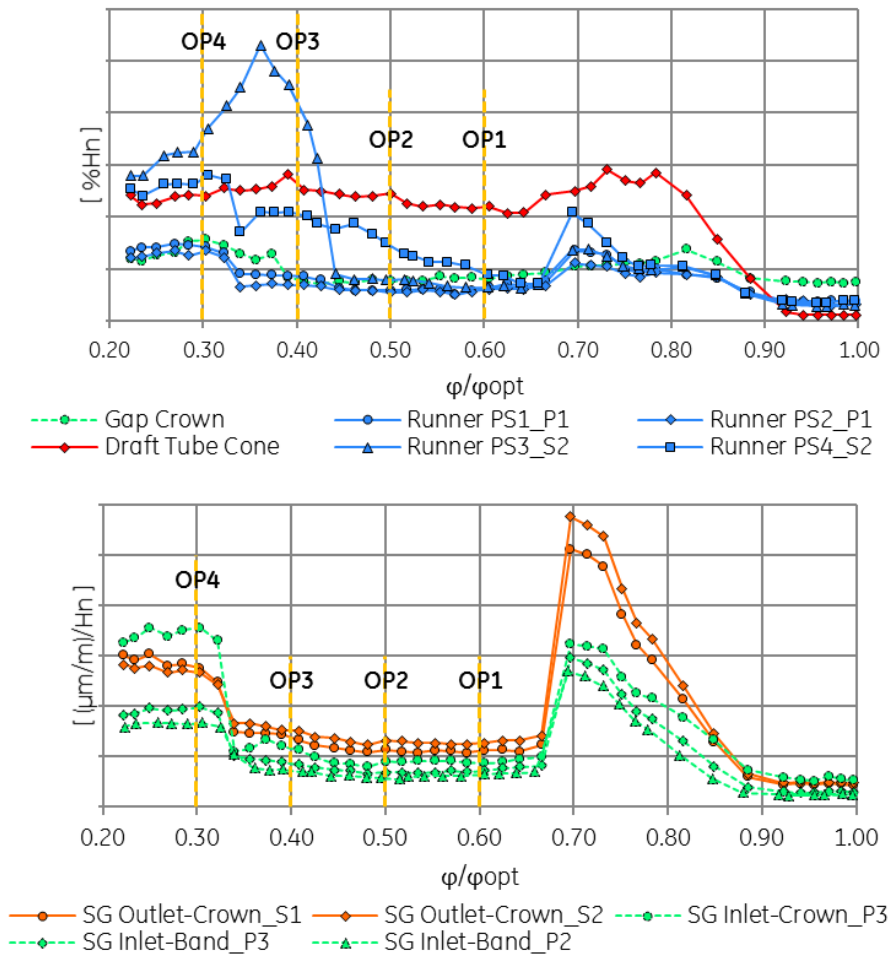


Figure 4 : Evolution of fluctuations during a load variation: pressure fluctuations (top) and dynamic strain (bottom)

To understand the root cause of the evolution of fluctuations inside the machine, observations of the flow were conducted. Four operating points (OP1 to OP4) were defined, from 60% to 30% of the optimal discharge coefficient (**Figure 4**), and all observations were made at plant cavitation conditions. **Figure 5** shows the corresponding pictures for the four operating points: on the left the flow downstream the runner is depicted, while on the right, the runner inlet flow is represented.

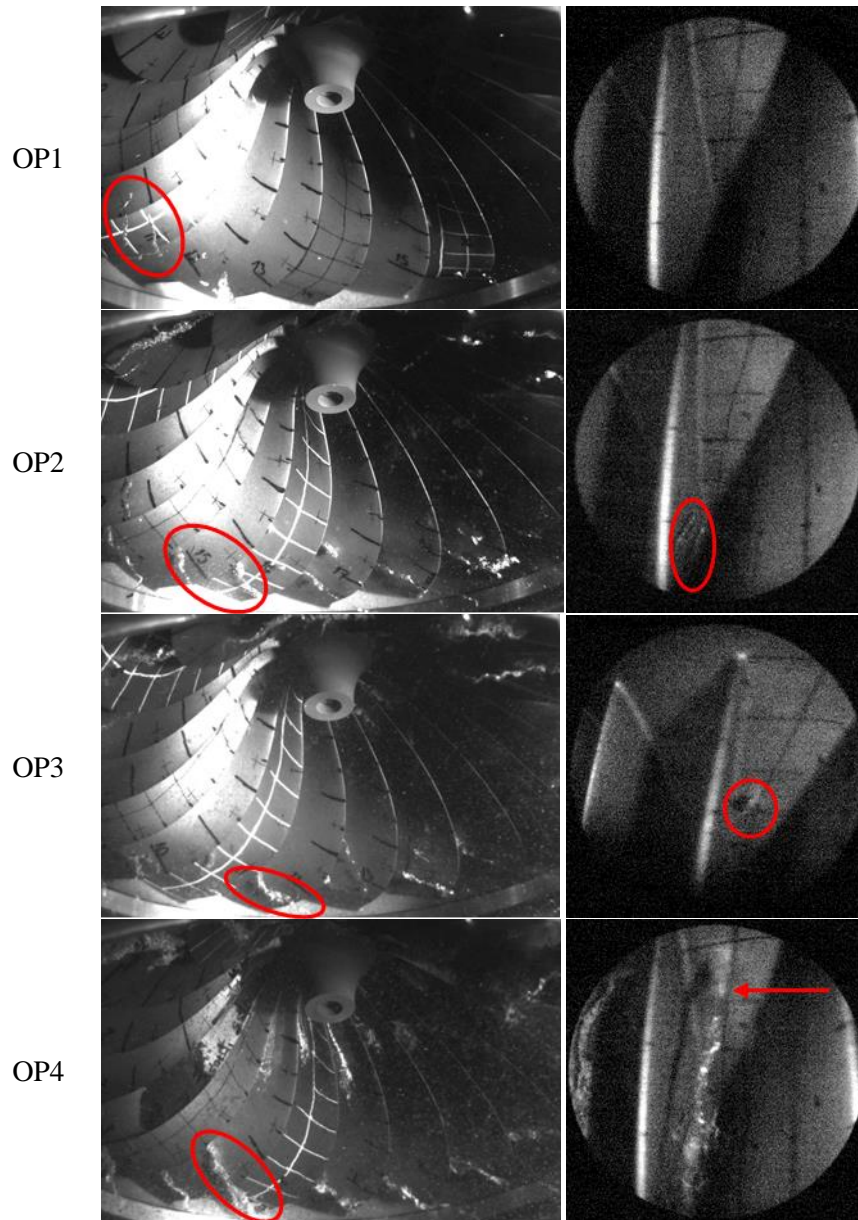


Figure 5: Inlet and outlet flow for OP1 to OP4

Concerning the incipient of inter-blade vortices, strain and pressure peak-to-peak levels were lower at OP1 compared to the vortex rope regime at $0.7\varphi_{opt}$. For this operating point, vortices began to appear at the runner outlet, close to the band as indicated on **Figure 5**. They were very unsteady and were present in only a few runner channels at the same time. Direct observation confirmed the presence of rotating vapor structures in the draft tube cone, interacting with inter-blade vortices. In this regime, reverse flow structures seem to reduce the local pressure below the blades suction side, thus cavitation forms in channel vortices core. The position of the vapor structures changes in time, as the flow rotates in the draft tube. Since stroboscopic lighting is used, the phenomenon is shifted to a new angular position at each flash, which is likely to give some stochastic aspect to the vortices in observers' eyes.

From OP1 to OP2, inter-blade vortices gained in strength. Outlet vortices appeared in all the runner channels, close to the band and seemed to be more steady and developed than for OP1 (it is worth to mention again that these observations were made with stroboscopic lighting). Seen from the guide vanes, several vortices started to appear in the middle of the runner channels, attached to the crown at 54% of the filet length from the leading edges and close to blades suction side.

From OP2 to OP3, both runner pressure sensors located on the inlet suction side of the instrumented blade measured higher peak-to-peak amplitudes. The same phenomenon developed at the runner outlet. The vortices gained strength and appeared thicker and longer. At the channel inlet, the vortex structures moved upstream and were then attached to the crown at 27% of the filet length from the leading edges. As such vortices get closer to suction side on-board sensors, they may disturb the local pressure field and induced the measured rise of fluctuations. As no vapor appeared any closer of these pressure sensors, it was not possible to visualize the actual flow field. Meanwhile, no significant increase of mechanical dynamic loading was observed.

From OP3 to OP4, pressure and strain fluctuations significantly increase, with the exception of the cone and one of the runner pressure sensors. The poor correlation between draft tube peak-to-peak pressure fluctuations and the dynamic strain experienced by the runner was found once again [3]. The same hydraulic structures continued to develop at channels outlet. At the inlet, large vortices arose from the crown to the bottom of the camera frame, at 14% of the filet length from blades leading edge. They appeared attached to the crown and their position varied between the middle of the channel and blades suction side. Further investigations are required to determine to what extent observed phenomena are linked to the increase of dynamic loading at OP4. Spectral analyses of strain and pressure signals for different cavitation conditions are currently ongoing.

For this load variation, the highest peak-to-peak level of strain fluctuations measured below $0.7\varphi_{opt}$ was found at OP4. Pressure fluctuations also rose in the vaneless area and for most of runner pressure sensors. Meanwhile, inter-blade vortices changed of shape from OP3 to OP4. Therefore, further investigations are conducted using numerical simulations to understand the flow field inside the runner at OP4.

3. NUMERICAL SETUP

In this study, a commercial finite volume solver was used to compute unsteady RANS calculations for the operating point OP4. The calculation domain consisted of three connected domains: the 24 guide vanes flow passages, the whole runner and the draft tube. At the outlet of the domain, an extension was placed to reduce the influence of the boundary conditions on the flow (**Figure 6**). Structured meshes were used for all domains. As investigations focus on the inter-blade vortices flow, the draft-tube mesh was coarser than the rest of the meshes (**Table 1**).

Domain	Number of nodes [10^6]	y_{max}^+
Distributor	3.8	4.5
Runner	8.0	6.2
Draft Tube	1.2	280

Table 1: Number of nodes and corresponding y^+ values

Transient Rotor-Stator interfaces were used to connect the three domains. At the inlet, the mass flow was prescribed according to the measurements at OP4. The angle of the inlet flow was defined by preliminary steady calculations of the tandem cascade. A 5% inlet turbulence intensity was chosen, and the eddy length scale was set to 10% of the distributor height. At the outlet, the average static pressure was set constant. The scale-resolving SAS-SST turbulence model was used. The selected time step was chosen to have 20 iterations per inter-blade channel, and corresponded to a rotation of roughly 1° of the runner. A sufficient number of inner loops were chosen for each time step, to ensure that the transient terms converge.

Additional monitoring points were placed and the evolution of pressure was recorded during the transient simulation. Their locations correspond to the reduced scale model pressure sensors in order to compare to the measurements. Experimental grid patterns were reproduced at the post-processing stage, to help the comparison of inter-blade vortices positions in the runner channels (**Figure 7**).

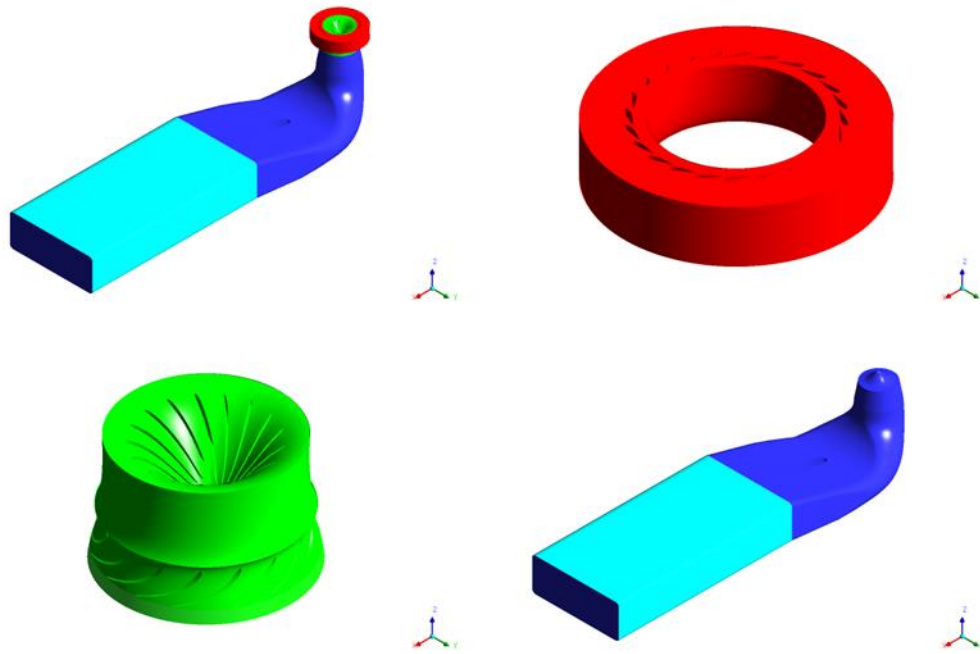


Figure 6: Calculation domain: Distributor (red), runner (green), draft tube (blue) and numerical extension (light blue)



Figure 7: Position of the monitoring points

4. NUMERICAL SIMULATIONS: COMPARISON WITH EXPERIMENTAL DATA

During the setup of the numerical simulations, only the flow rate through the machine, the runner rotation speed and the guide vanes opening were given as boundary conditions. Thus, the discharge coefficient φ was ensured during the calculations. However, the net head remained a result of the simulation and the energy coefficient was underestimated by around 6% compared to the targeted operating point OP4. The torque coefficient was underestimated by around 9%. Based on the measured hill chart of the machine, this difference is not expected to induce significant modification of the flow features.

4.1 Flow analysis

On **Figure 8**, time-averaged velocity streamlines and pressure field on the crown are represented. Light blue streamlines are coming from the runner inlet, while red streamlines are coming from the runner outlet, both flowing near the crown. It can be concluded from the front view of the runner that upstream and downstream flows are interacting near the crown, and mixing in the inter-blade vortices. The reverse flow mechanism can be observed here, as the flow enters runner channels outlet. Local minimums of time-averaged pressure can be seen on the crown, which correspond to the core of the attached vortices (as seen on **Figure 5** at OP4). Their locations are in good agreement with experimental observations at 14% of the fillet length from leading edges, between the middle of the channel and blade suction side (see location on grid pattern).

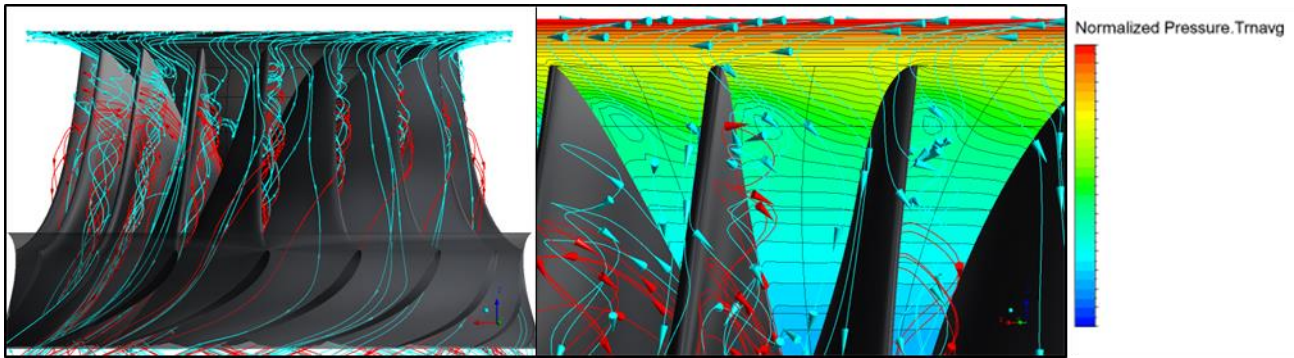


Figure 8: Time-averaged velocity streamlines near the crown, from upstream (light blue) and downstream (red), and time-averaged pressure field on the crown

On **Figure 9**, instantaneous velocity and pressure fields are shown. In addition, surfaces of constant Q -criterion restricted to positive axial vorticity is displayed. Whilst the time-averaged velocity and pressure fields appeared quite axisymmetric (**Figure 8**), the obtained unsteady flow exposes different vortices in each runner channel, and consequently the pressure on the crown. Both the upstream and downstream flows merge in spanwise coherent structures that are rotating in the same direction as the runner, as experimentally observed at OP4 (**Figure 5**).

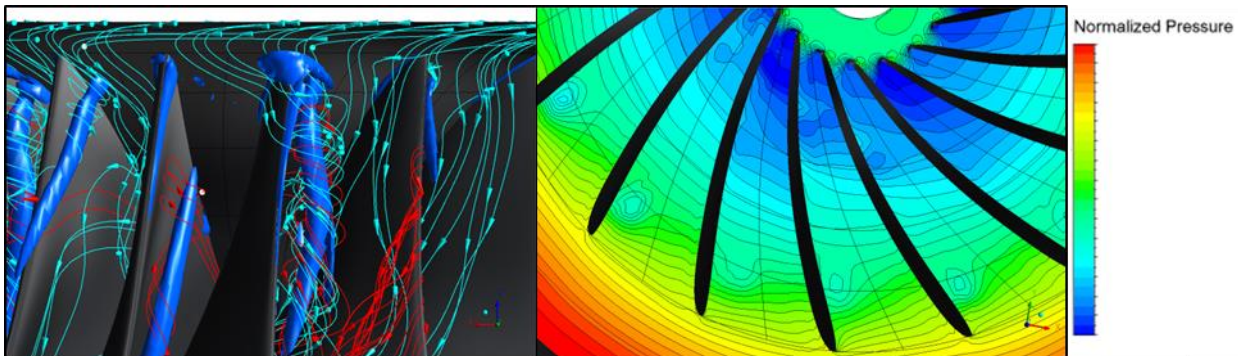


Figure 9: Iso-surface of Q -criterion restricted to positive axial vorticity (right). Instantaneous velocity streamlines and pressure contours on the crown (left).

Upstream-downstream interactions can also be observed in 2D representations. On **Figure 10**, circumferentially averaged streamwise velocity is displayed on the runner meridional plane. As it can be seen, the pumping flow encounters the upstream flow close to the crown. The dashed line represents the circumferentially averaged limit between the main and reverse flows in the runner channels (where the velocity has no streamwise component). At the runner inlet, there is less flow near the crown than at the band. Consequently, the velocity level is reduced in the crown area. As a result, the provided flow angle is poorly adapted at the leading edge, as can be seen from the blade-to-blade view (**Figure 10**). One part of the flow is blocked on the pressure side (where the flow tends to hit the blades), whereas the other part accelerates when it passes around the leading edge and goes to the suction side, where flow separation occurs. In this case, the separation forms a vortex structure that is creating a local minimum of pressure at the crown surface previously mentioned. Downstream, the flow passages are blocked near the crown and both main and reverse flows degenerate into 3D vortex structures, which are finally convected by the discharge near the band, thus forming inter-blade vortices.

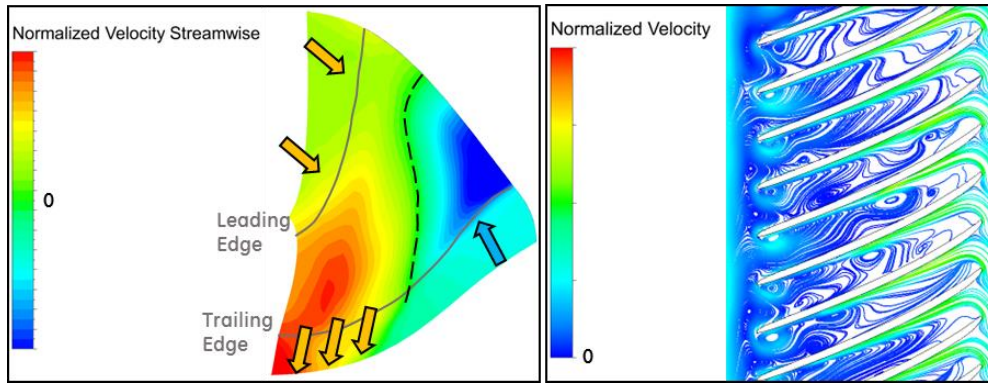


Figure 10: Circumferentially averaged instantaneous streamwise velocity in the runner meridional plane (left) and instantaneous surface streamlines near the crown on a 10% normalized span Blade-to-Blade surface (right)

4.2 Predicted pressure fluctuations and comparison to measurements

Transient statistics were recorded for the pressure field for more than 50 runner revolutions, to ensure the convergence of statistical quantities. On **Figure 11** the standard deviation of the pressure on the crown and on the blades is depicted. From the top view of the runner, it can be seen on the crown a region of locally increased fluctuations at 14% of the filet length from the leading edge (dashed circles). On the front view, this fluctuating region expands also on the blades on both the pressure and suction sides (between dashed lines), where runner sensors PS3_S2 and PS4_S2 were positioned. As mentioned before, this is due to the development of inter-blade vortices. Furthermore, on the meridional view of the runner (**Figure 11**), the circumferential-average of the pressure standard deviation shows a maximum between the leading edge and the zero streamwise velocity limit (as on **Figure 10**). It suggests that the inter-blades vortices generate a local increase of the pressure fluctuations that are numerically predicted inside runner channels.

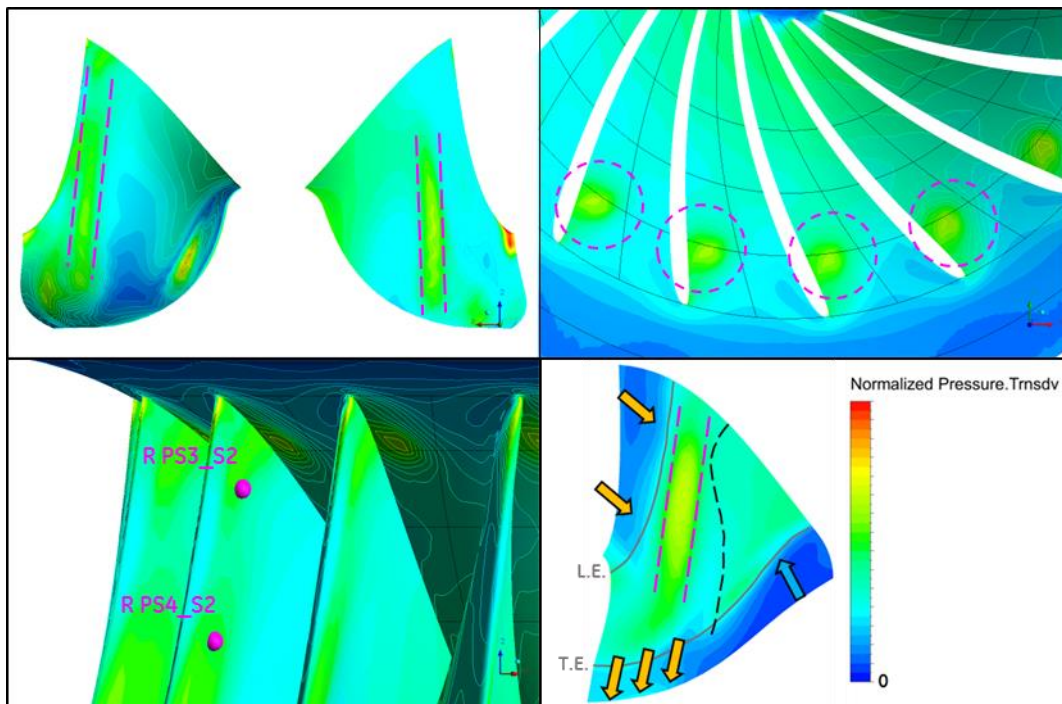


Figure 11: Pressure standard deviation on the runner and the circumferential-averaged pressure on the meridional plane.

Pressure fluctuations levels at the monitoring points are compared to the measurements in the vaneless area, the runner and the draft tube. On **Figure 12**, predicted peak-to-peak values of pressure signals reach the same order of magnitude as the experimental results at OP4, for all the sensors. The prediction errors are -22%, +43% and +12% for the sensor in the vaneless area, in the runner and in the draft tube respectively, and the time evolution of the signals is coherent with the experimental data. Higher frequency phenomena found in the measures was not predicted. Thus, further spectral analyses are required, and numerical pressure

spectra will be compared to experimental ones. Such high frequencies that are not present may be due to smaller scales not correctly resolved with the present mesh: a finer grid refinement will be necessary. A next step would be to test also a cavitation model, to check if it has an impact on the accuracy for predicting pressure fluctuations amplitude and frequencies linked to these cavitating inter-blade-vortices.

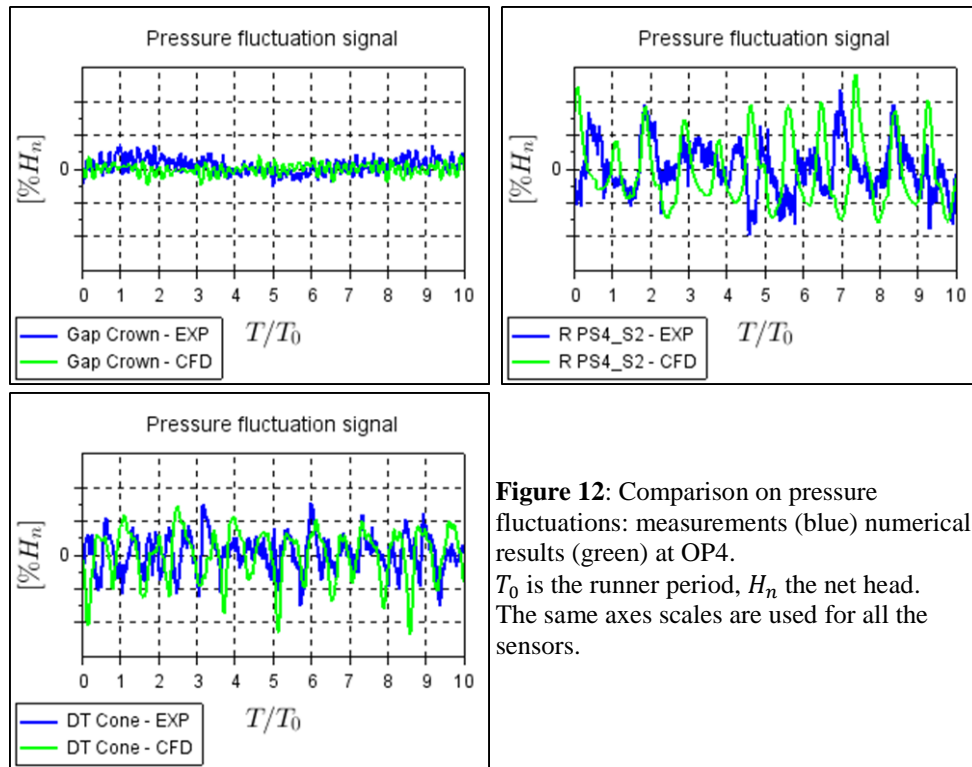


Figure 12: Comparison on pressure fluctuations: measurements (blue) numerical results (green) at OP4. T_0 is the runner period, H_n the net head. The same axes scales are used for all the sensors.

5. CONCLUSION

In this study, deep partial load inter-blade vortices were studied using both experimental and numerical approaches. An instrumented reduced scale model turbine was tested, which allowed strain and pressure fluctuations to be correlated to the high-speed visualizations of the flow inside the runner. One deep partial load operating point was chosen to perform URANS calculations, and the experimental data were essential to assess the suitability of the numerical modeling. The predicted flow field was in good agreement with the observations, especially concerning the position of the inter-blade vortices inside the runner channels. Further insights of the vortices development highlighted complex interactions between upstream and downstream flows when they mix inside the runner. The predicted standard deviation of the pressure field gave coherent qualitative results, as fluctuating regions were found close to the inter-blade vortices locations. Nonetheless, the obtained pressure signals could be improved, as higher frequencies might have been underestimated by the numerical model. Therefore, further investigations are needed to reproduce more accurate pressure spectra on the runner.

Such pressure fluctuations are required to foresee the dynamic mechanical loading on the runner in deep partial load conditions. Both experimental and numerical approaches provide helpful information on the impact of inter-blade vortices on Francis turbine runners, and help to better understand the flow behavior in off-design operating conditions.

ACKNOWLEDGEMENTS

The present work was funded by the French Directorate General for Enterprise. The authors acknowledge GE Renewable Energy for providing the data and techniques of the Global Technology Center, in Grenoble.

REFERENCES AND CITATIONS

- [1] J. Brammer, F. Duparchy, P. Y. Lowys, M. Thibaud, K. Wheeler et T. De Colombel, «Increasing the operating range of Francis turbines by considering dynamic phenomena at partial load,» *Proc. of the Hydro 2016 conference*, 2016.
- [2] P.-Y. Lowys, F. Paquet, M. Couston, M. Farhat, S. Natal et F. Avellan, «Onboard Measurements of Pressure and Strain Fluctuations in a Model of Low Head Francis Turbine - Part 2 : Measurements and Preliminary Analysis Results,» *Proc. of the 21st IAHR Symp., Hydraulic Machinery and Systems*, vol. II, pp. 873-880, 2002.
- [3] F. Bouloc, J. Guillozet, F. Duparchy, P. Y. Lowys et A. Duparchy, «Mechanical risks prediction on Francis runner by Spatial Harmonic Decomposition,» *Proc. of the 28th IAHR Symp. on Hydraulic Machinery and Systems*, pp. 703-712, 2016.
- [4] S. Bouajila, T. De Colombel, P. Y. Lowys et T. Maître, «Hydraulic phenomena frequency signature of Francis turbines operating in part load conditions,» *Proc. of the 28th IAHR Symp. on Hydraulic Machinery and Systems*, pp. 1281-1290, 2016.
- [5] J. P. Franc, F. Avellan, B. Belahadji, J. Y. Billard, L. Briançon-Marjollet, D. Fréchou, D. H. Fruman, A. Karimi, J. L. Kueny et J. M. Michel, *La cavitation - Mécanismes physiques et aspects industriels*, 1995.
- [6] L. Zhou, M. LIU, Z. Wang, D. LIU et Y. ZHAO, «Investigation of Channel Vortices in Francis Turbines,» *Proc. of the 28th IAHR Symp. on Hydraulic Machinery and Systems*, pp. 1301-1310, 2016.
- [7] M. V. Magnoli, «Comparison of model measured runner blade pressure fluctuations with unsteady flow analysis predictions,» *Proc. of the 28th IAHR Symp. on Hydraulic Machinery and Systems*, pp. 1291-1300, 2016.
- [8] K. Yamamoto, A. Müller, A. Favrel, C. Landry et F. Avellan, «Numerical and experimental evidence of inter-blade cavitation vortex development at deep part load operation of a Francis turbine,» *Proc. of the 28th IAHR Symp. on Hydraulic Machinery and Systems*, pp. 1323-1330, 2016.
- [9] I. E. Comission, *Hydraulic turbines, storage pumps and pump-turbines - Model acceptance test (Int. Standard IEC 60193)*, 1999.
- [10] K. Yamamoto, A. Müller, A. Favrel, C. Landry et F. Avellan, «Guide Vanes Embedded Visualization technique for Investigating Francis Runner Inter-blade Vortices at Deep Part Load Operation,» *Proc. of the 6th IAHR Int. Meeting of the Workgroup on Cavitation and Dynamic Problems in Hydraulic Machinery and Systems*, 2015.